Chapter 6

BOOSTED OBJECT RECONSTRUCTION

After a detailed exposition of the various reconstruction techniques in **??**, further selections and quality criteria are applied to define a set of baseline and candidate reconstructed objects that will be used in the analysis and the kinematic variables to discriminate between signal and background and maximize the sensitivity for a discovery of new physics. An introduction to estimating the size parameter of large radius jets is described in section 6.1. The rest of this brief chapter describes in detail the further selections on the reconstructed objects for: jets (section 6.2.1), b-tagged jets (section 6.2.2), leptons[1] (section 6.2.3), the procedure for removing energy overlaps in the reconstructed objects (section 6.2.4), large radius reclustered jets (section 6.2.5), and the reconstructed missing transverse momentum (section 6.2.6).

6.1 Size of Boosted Jets

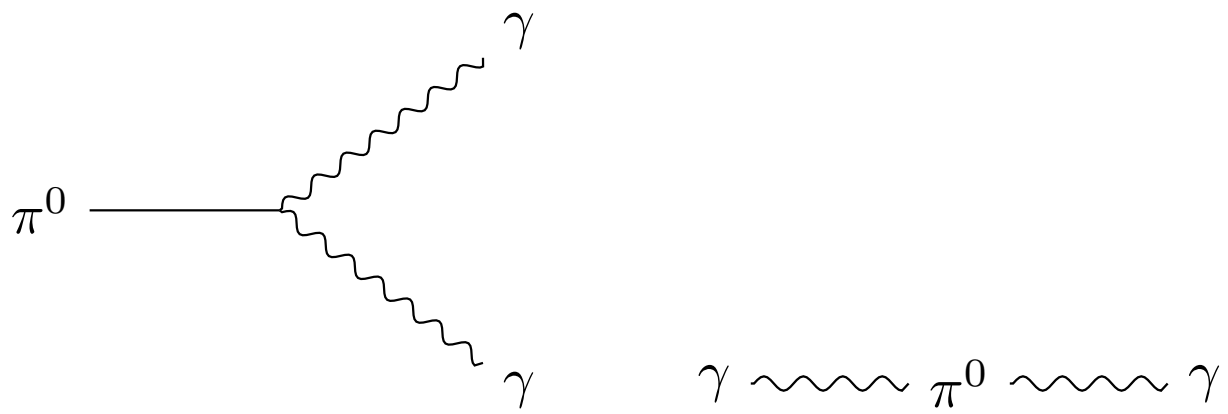

(a) lab frame (b) rest frame

Figure 6.1: A feynman diagram of the two-body decay of a neutral pion π^0 to two photons γ in the (a) lab frame and (b) rest frame.

[1]The term "lepton" exclusively refers to electron or muon in this thesis.

Consider a two-body relativistic decay as shown in fig. 6.1 with $m_{\pi^0} \gg m_\gamma = 0$. The question one might pose is: *What is the opening angle between the two photons?* Since a (real) photon has no mass, its energy and momentum are the same $E_\gamma = |\vec{p}_\gamma|$. To transform between the lab frame (LAB) and the rest frame (RF) of the π^0, the boost is described along z by $\gamma = \frac{E_{\pi^0}}{m_{\pi^0}}$ and $\beta = v_{\pi^0} = \frac{|\vec{p}_{\pi^0}|}{E_{\pi^0}}$. Applying this boost to each photon (denoted by $\pm$) to transform from the rest frame to the lab frame, we find in each component

$$E^{\text{LAB}}_{\pm,\parallel} = \gamma(E^{\text{RF}}_{\parallel} \pm \beta E^{\text{RF}}) = \frac{1}{2}\gamma m_{\pi^0} \tag{6.1}$$

$$E^{\text{LAB}}_{\perp} = E^{\text{RF}}_{\perp} = \frac{1}{2} m_{\pi^0} \sin\theta^{\text{RF}} \tag{6.2}$$

where θ^{RF} is the angle that the photon makes with the z-axis and $E_\parallel, E_\perp$ refer to a longitudinal and perpendicular component of the γ energy with respect to the momentum of the neutral pion. Therefore, the total energy of the photons in the lab frame is sum in quadrature

$$E^{\text{LAB}}_{\pm} = \frac{1}{2} m_{\pi^0} \sqrt{\gamma^2(\cos\theta^{\text{RF}} \pm \beta)^2 + \sin^2\theta^{\text{RF}}} = \frac{1}{2} m_{\pi^0}(1 \pm \beta\cos\theta^{\text{RF}}) \tag{6.3}$$

Unfortunately, the algebra starts to get a little bit hairy, so it is surprisingly useful to define

$$g = \left|\frac{E_+ - E_-}{E_+ + E_-}\right| = \beta\cos\theta^{\text{RF}} \tag{6.4}$$

which simplifies eq. (6.3) so that we get $E^{\text{LAB}}_{\pm} = \frac{1}{2} m_{\pi^0}(1 \pm g)$. So to determine the angle θ between the photons, we calculate the 4-vector of the total system

$$m_{\pi^0}^2 = (\gamma_+ + \gamma_-)^2 = 2E_+E_- - 2E_+E_- \cos\theta \qquad \Rightarrow \qquad \cos\theta = \frac{2E_+E_- - m_{\pi^0}^2}{2E_+E_-}. \quad (6.5)$$

This equation can then simplify down to

$$\begin{aligned} \cos\theta &= \frac{\gamma^2(1-g^2)-2}{\gamma^2(1-g^2)} = \frac{\gamma^2(\beta^2-g^2)-1}{\gamma^2(1-g^2)} = \frac{E_{\pi^0}^2(1-g^2)-2m_{\pi^0}^2}{E_{\pi^0}^2(1-g^2)} \\ &= 1 - \frac{2m_{\pi^0}^2}{E_{\pi^0}^2(1-g^2)} \end{aligned} \quad (6.6)$$

where the identity $\gamma^2 - \beta^2\gamma^2 = 1$ is used. Now, a "small-angle approximation" is used in the case of a boosted regime where the photons are collimated in the lab frame. This allows us to further simplify eq. (6.6). In small $g \to 0, \theta$, we can expand θ out

$$\cos\theta \approx 1 - \frac{1}{2}\theta^2 = 1 - \frac{2}{\gamma^2} \quad (6.7)$$

and this gives us $\theta = \frac{2}{\gamma}$, or as more commonly known among experimental physicists in ATLAS

$$\Delta R \sim \frac{2m}{p_{\mathrm{T}}} \quad (6.8)$$

What this equation tells us is that the higher the p_{T} of a parent particle (such as a neutral pion or a top quark), the smaller the opening angle, the smaller the ΔR between decay particles, and the more collimated the particles are. It turns out that this works very well in

practice, as shown in fig. 6.2 for $Z' \to t\bar{t}$ decays where the angular separation is shown as a function of the parent particle in a 2-body decay for the top quark decay and the hadronic W boson decay. It is here that one can see for $p_{\mathrm{T}}^{\mathrm{top}} > 350\,\mathrm{GeV}$, the decay products of the top quark tend to have a separation of $\Delta R < 1.0$. As will be described in the next section, this technique is effective for capturing the full decay of boosted objects with significant substructure inside a single large radius jet.

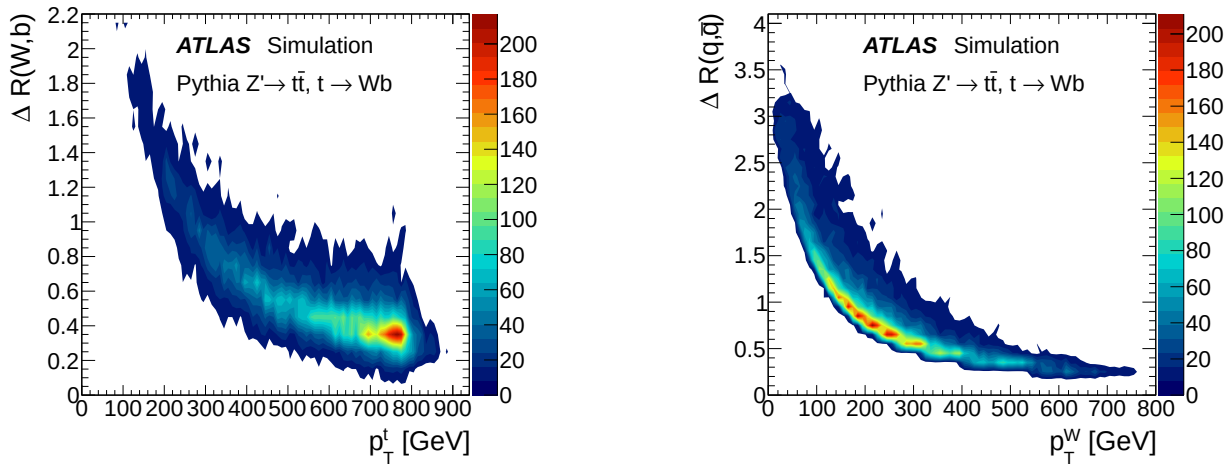

(a) $\Delta R(W, b)$ (b) $\Delta R(q, \bar{q})$

Figure 6.2: [1] The angular separation between the (a) W boson and b-quark in top decays and (b) light quarks in W boson decays as a function of the p_{T} of the parent particle. Both distributions are at the generator level and do not include effects due to initial and final-state radiation, or the underlying event.

6.2 Objects

This section will detail the definitions of objects used in the analysis from the perspective of the physics of the detector. Corrections derived from data control samples are applied to simulated events to account for differences between data and simulation in the reconstruction efficiencies, momentum scale and resolution of leptons[2], in the efficiency and fake rate for

[2]The term "lepton" exclusively refers to electron or muon in this thesis.

identifying b-jets, and in the efficiency for rejecting jets originating from pile-up interactions.

Interaction vertices from the proton–proton collisions are reconstructed from at least two tracks with $p_{\mathrm{T}}^{\mathrm{track}} > 0.4\,\mathrm{GeV}$, and are required to be consistent with the beamspot envelope. The primary vertex is identified as the one with the largest sum of squares of the transverse momenta from associated tracks [2]

$$\sum {p_{\mathrm{T}}^{\mathrm{track}}}^2. \tag{6.9}$$

Identifying the primary vertex is also important to mitigate pile-up contamination in the calculation of $E_{\mathrm{T}}^{\mathrm{miss}}$.

A series of basic selection critera are applied to electrons, muons, and jets to define the baseline candidates for an event. From these objects, an overlap removal procedure is applied to prevent double-counting. More stringent requirements are then applied to the overlap-removed, baseline objects to select the final candidates that will be used for the calculation of the kinematic observables in **??**. The details of the object selections and overlap removal procedure is given below in more detail.

6.2.1 Small-radius jets

Small-radius (small-R) jets[3] are objects that have been reconstructed from three-dimensional topo-clusters [3] in the hadronic and electromagnetic calorimeters using the anti-k_t jet algorithm [4, 5] with a radius parameter of $R = 0.4$. Before we can make use of these jets, they need to be properly calibrated to compensate and account for reconstruction-based

[3]Unless otherwise specified, "jets" will always refer to the candidate, overlap-removed (see section 6.2.4), small-R jets.

limitations such as:

- dead material: energy lost in the dead material of the detector, e.g. inactive absorbers and instrumentation
- non-compensation: difference in detector response between hadrons, leptons, and photons; specifically the response is lower for hadrons
- punch-through: energy leakage where the hadron showers deposit energy outside of the calorimetry system
- pile-up: energy originating from additional proton-proton collisions in the detector (part of the underlying event which includes initial and final state radiation)
- minimum threshold: hardware limits on energy deposits
- out-of-cone: inefficiencies in reconstruction due to not capturing the full particle shower in the jet

Each topo-cluster is calibrated to the electromagnetic scale response prior to jet reconstruction. The reconstructed jets are then calibrated to the particle level by the application of a jet energy scale (JES) derived from $\sqrt{s} = 13\,\text{TeV}$ data and simulations [6]. Quality criteria are imposed to reject events that contain at least one jet arising from non-collision sources or detector noise [7]. Further selections are applied to reject jets that originate from pile-up interactions by means of a multivariate algorithm, jet-vertex-tagger (JVT) [8], using information about the tracks matched to each jet [9]. For jets with $p_{\text{T}}^{\text{jet}} < 60\,\text{GeV}$ and located centrally in the detector, where pile-up jets are prominent, we require JVT > 0.59. The baseline jets are required to have $p_{\text{T}}^{\text{jet}} > 20\,\text{GeV}$ and $|\eta| < 2.8$. After resolving overlaps with baseline leptons (electrons and muons), candidate jets are a subset of the baseline jets that have no overlaps and a stricter cut on transverse momentum, $p_{\text{T}}^{\text{jet}} > 30\,\text{GeV}$.

6.2.2 *b-tagged jets*

From the candidate jets described in section 6.2.1, we apply a multivariate b-tagging algorithm, `MV2c10`, using information about the [10, 11]

- impact parameters of inner detector tracks matched to the jet
- presence of displaced secondary vertices
- reconstructed flight paths of b-hadrons and c-hadrons inside the jet

Of the candidate jets, we require a tighter cut on $p_{\mathrm{T}}^{\mathrm{jet}} > 30\,\mathrm{GeV}$ with $|\eta| < 2.5$ as this is the region of the calorimeter where the Inner Detector (ID) provides tracking information. The `MV2c10` algorithm provides a discriminant which a selection is applied on to provide a specific efficiency for the b-tagging algorithm. In this analysis, a working point was chosen corresponding to an efficiency of 77%, determined from a sample of simulated $t\bar{t}$ events[4]. This working point was found to be optimal for the statistical significance of the search for a majority of the phase-space, compared to the 60%, 70%, and 85%[5] working points.

6.2.3 *Leptons*

All baseline leptons are required to have $p_{\mathrm{T}} > 20\,\mathrm{GeV}$ along with the specified identification and quality criteria[6]. Baseline electrons are reconstructed from energy clusters in the electromagnetic calorimeter (EMCal) and ID tracks. These electrons are required to have

[4] At the 77% working point, the corresponding rejection factors against jets originating from c-quarks, τ-leptons, and light quarks & gluons are 6, 22, and 134 respectively. [12]

[5] The optimization did sometimes favor the 85% working point, but 77% was not significantly worse. On top of this, there are some benefits using a lower efficiency working point for background estimation due to the enhanced purity of the flavor composition.

[6] The muon and electron definition choices were optimized in the previous version of the analysis [13].

$|\eta| < 2.47$ and pass a set of "loose" quality and identification criteria [14, 15]. Baseline muons are reconstructed from matching tracks in the ID and muon spectrometer. These muons are required to have $|\eta| < 2.5$ and pass a set of "medium" quality and identification criteria [16].

Leptons are selected from the candidates that survive the overlap removal procedure if they fulfill a requirement on the $\sum p_{\mathrm{T}}^{\mathrm{track}}$ of additional ID tracks in an "isolation" cone around the lepton track. This isolation requirement is defined to ensure a flat efficiency of around 99% across the whole electron transverse energy and muon transverse momentum ranges.

The angular separation between the lepton and the b-jet ensuing from a semileptonic top quark decay narrows as the p_{T} of the top quark increases. This increased collimation is taken into account by continuously changing the radius of the isolation cone on an event-by-event basis as

$$\min_{\text{leptons}} \left(0.2, \frac{10\,\mathrm{GeV}}{p_{\mathrm{T}}^{\mathrm{lep}}} \right), \tag{6.10}$$

where $p_{\mathrm{T}}^{\mathrm{lep}}$ is the lepton p_{T} expressed in GeV.

Selected electrons are further required to meet the "tight" quality criteria [14, 15]. Selected muons do not have tightened quality criteria. Leptons are matched to the primary vertex by requiring the transverse impact parameter d_0 of the associated ID track to satisfy

$$\left| \frac{d_0}{\sigma_{d_0}} \right| < 5 \qquad \text{for electrons and} \tag{6.11a}$$

$$\left| \frac{d_0}{\sigma_{d_0}} \right| < 3 \qquad \text{for muons,} \tag{6.11b}$$

where σ_{d_0} is the measured uncertainty of the transverse impact parameter. The longitudinal

impact parameter z_0 is required to satisfy

$$|z_0 \sin\theta| < 0.5\,\text{mm}. \tag{6.12}$$

Both the transverse d_0 and longitudinal z_0 impact parameters are defined with respect to the selected primary vertex.

6.2.4 Overlap Removal

In order to make sure the event is reconstructed accurately, one needs to account for double-counting of energy in the detector. For example, if a high-p_{T} muon radiates some energy in the hadronic calorimeter and then is subsequently captured by the muon spectrometer. I could reconstruct a jet with very few ID tracks and detect a muon, but this jet is formed from final state radiation rather than as part of the hadronization of the parton shower so I should remove this "jet" if it "overlaps" with the muon. Steps are taken to remove "fake" objects as well as energy overlap in the ATLAS detector.

Objects are considered to overlap if they lie less than a distance ΔR from each other

$$\Delta R = \sqrt{(\Delta\eta)^2 + (\Delta\phi)^2} \tag{6.13}$$

where ΔR defines the distance in rapidity y and azimuthal angle ϕ. Overlaps between candidate objects are removed sequentially. The overall procedure is as follows:

1. Electron-Muon: Overlaps between electron and muon candidates are removed. Only electrons get removed at this stage.

2. Electron-Jet: Overlaps between electron and jet candidates are removed. Both electrons and jets can get removed at this stage.

3. Muon-Jet: Overlaps between remaining jets and muon candidates are removed. Both muons and jets can get removed at this stage.

Electron candidates that lie a distance $\Delta R < 0.01$ from muon candidates are removed to suppress contributions from muon bremsstrahlung.

Overlap removal between electron and jet candidates aims to resolve two sources of ambiguity:

1. remove jets that are formed primarily from the showering of a prompt electron; and
2. remove electrons that are produced in the decay chains of hadrons.

Consequently, any non-b-tagged jet whose axis lies $\Delta R < 0.2$ from an electron is discarded. Electrons with $E_{\mathrm{T}} < 50\,\mathrm{GeV}$ are discarded if they lie $\Delta R < 0.4$ from the axis of any remaining jet and the corresponding jet is kept. For higher E_{T} electrons, the latter removal is performed using a variable threshold

$$\Delta R = \min\left(0.4, 0.04 + \frac{10\,\mathrm{GeV}}{E_{\mathrm{T}}^{\mathrm{electron}}}\right) \tag{6.14}$$

to increase the acceptance for events with collimated top quark decays[7].

Overlap removal between muon and jet candidates aims to resolve two sources of ambiguity:

1. remove jets[8] that appear in close proximity to muons due to high-p_{T} muon bremsstrahlung while retaining the overlapping muon; and

[7] If you have a very boosted top quark, you often have a real electron close to a real b-jet. This is why both the electron and b-tagged jet would be kept.

[8] These jets usually have very few matching ID tracks.

2. remove muons that are likely to have originated from the decay of hadrons while retaining the overlapping jet.

If the angular distance between a muon and a jet is small, $\Delta R < 0.2$, the jet is removed if it is not b-tagged and has fewer than three matching ID tracks. Muons overlapping with remaining jets are removed if

$$p_{\mathrm{T}}^{\mathrm{muon}} < 50\,\mathrm{GeV} \quad \text{and} \quad \Delta R < 0.4 \quad \text{or} \tag{6.15a}$$

$$p_{\mathrm{T}}^{\mathrm{muon}} > 50\,\mathrm{GeV} \quad \text{and} \quad \Delta R < \min\left(0.4, 0.04 + \frac{10\,\mathrm{GeV}}{p_{\mathrm{T}}^{\mathrm{muon}}}\right) . \tag{6.15b}$$

6.2.5 Large-radius jets

The overlap-removed, candidate jets described in section 6.2.1 are re-clustered [17, 18] into large-radius (large-R) jets[9] using the anti-k_t jet algorithm [4, 5] with a radius parameter of $R = 0.8$. Unlike regular large-R jets formed from topo-clusters and require a separate set of calibrations, the small-R jet calibrations[10] directly propagate through to the re-clustered large-R jets, eliminating the need to prepare specific calibration for each large-R jet collection considered for use in an analysis. These re-clustered jets are further groomed [19, 17, 1, 20] using a trimming[11] algorithm with $f_{\mathrm{cut}} = 0.1$. Candidate large-R jets are required to have $p_{\mathrm{T}}^{\mathrm{jet}} > 100\,\mathrm{GeV}$ and $|\eta| < 2.0$. The radius R and trimming parameter f_{cut} were optimized in the previous version of the analysis [13]. Scanning over $R = 0.8, 1.0, 1.2$ with $f_{\mathrm{cut}} = 0.05, 0.10, 0.20$, the expected sensitivity of the analysis was maximized with $R =$

[9] Unless otherwise specified, "large-R" jets will always refer to the candidate, re-clustered, trimmed jets.

[10] The jet energy scale (JES) uncertainties are used to describe the mass uncertainty on the reclustered jets. In the signal regions, less than 2% of these reclustered jets were formed from a single small-R jet, so the mass of the reclustered jet originates from the $p_{\mathrm{T}}^{\mathrm{jet}}$ and separation between small-R jets.

[11] Trimming for re-clustered jets means to remove subjets where $p_{\mathrm{T}}^{\mathrm{subjet}} < f_{\mathrm{cut}} p_{\mathrm{T}}^{\mathrm{jet}}$. For this analysis, subjets with $p_{\mathrm{T}} < 10\%$ of the re-clustered $p_{\mathrm{T}}^{\mathrm{jet}}$ were removed.

0.8, $f_{\text{cut}} = 0.1$. Therfore, any variable that can be constructed from these large-R jets to take advantage of the high likelihood for a contained top quark in each reclustered jet will become a powerful variable to discriminate signal (four tops) over background (zero, one, and two tops).

6.2.6 Missing Transverse Momentum

The $E_{\text{T}}^{\text{miss}}$ in the event is defined as the magnitude of the negative vector sum ($\vec{p_{\text{T}}}^{\,\text{miss}}$) of the transverse momenta of all selected and calibrated baseline muons, electrons, and small-R jets in the event, with an extra "soft" term added to account for energy deposits that are not associated with any of these selected objects.

$$E_{\text{T}}^{\text{miss}} = \underbrace{-\sum \vec{p}_{\text{T}}}_{\text{baseline objects}} + \text{track soft term} \tag{6.16}$$

This "soft" term is calculated from ID tracks matched to the primary vertex to make it more resilient to contamination from pile-up interactions [21, 22].

Glossary

topo-cluster topological energy cluster. 5, 6, 11

EMCal electromagnetic calorimeter. 7

ID Inner Detector. 7–12

JES jet energy scale. 11

JVT jet-vertex-tagger. 6

large-R large-radius. 11, 12

punch-through For jets at very high transverse momentum it is possible that part of the energy is not deposited in the calorimeter, but leaks out to the detector components beyond the calorimeter. This leads to a systematic reduction in the measured jet energy. Jets that deposit energy beyond the hadronic Tile calorimeter and in the muon system are called punch-through jets. [23]. 6

small-R small-radius. 5, 11, 12

Bibliography

[1] ATLAS Collaboration. "Performance of jet substructure techniques for large-R jets in proton–proton collisions at $\sqrt{s} = 7$ TeV using the ATLAS detector". In: *JHEP* 09 (2013), p. 076. DOI: 10.1007/JHEP09(2013)076. arXiv: 1306.4945 [hep-ex] (cit. on pp. 4, 11).

[2] ATLAS Collaboration. *Vertex Reconstruction Performance of the ATLAS Detector at$\sqrt{s} = 13$ TeV*. ATL-PHYS-PUB-2015-026. 2015. URL: https://cds.cern.ch/record/2037717 (cit. on p. 5).

[3] ATLAS Collaboration. "Topological cell clustering in the ATLAS calorimeters and its performance in LHC Run 1". In: *Eur. Phys. J. C* 77 (2017), p. 490. DOI: 10.1140/epjc/s10052-017-5004-5. arXiv: 1603.02934 [hep-ex] (cit. on p. 5).

[4] Matteo Cacciari, Gavin P. Salam, and Gregory Soyez. "The anti-k_t jet clustering algorithm". In: *JHEP* 04 (2008), p. 063. DOI: 10.1088/1126-6708/2008/04/063. arXiv: 0802.1189 [hep-ph] (cit. on pp. 5, 11).

[5] Matteo Cacciari, Gavin P. Salam, and Gregory Soyez. "FastJet User Manual". In: *Eur. Phys. J. C* 72 (2012), p. 1896. DOI: 10.1140/epjc/s10052-012-1896-2. arXiv: 1111.6097 [hep-ph] (cit. on pp. 5, 11).

[6] ATLAS Collaboration. "Jet energy scale measurements and their systematic uncertainties in proton-proton collisions at $\sqrt{s} = 13$ TeV with the ATLAS detector". In: *Submitted to Phys. Rev. D* (2017). arXiv: 1703.09665 [hep-ex] (cit. on p. 6).

[7] ATLAS Collaboration. *Selection of jets produced in 13 TeV proton–proton collisions with the ATLAS detector*. ATLAS-CONF-2015-029. 2015. URL: https://cds.cern.ch/record/2037702 (cit. on p. 6).

[8] ATLAS Collaboration. *Tagging and suppression of pileup jets with the ATLAS detector*. ATLAS-CONF-2014-018. 2014. URL: https://cds.cern.ch/record/1700870 (cit. on p. 6).

[9] ATLAS Collaboration. "Performance of pile-up mitigation techniques for jets in pp collisions at $\sqrt{s} = 8$ TeV using the ATLAS detector". In: *Eur. Phys. J. C* 76 (2016), p. 581. DOI: 10.1140/epjc/s10052-016-4395-z. arXiv: 1510.03823 [hep-ex] (cit. on p. 6).

[10] ATLAS Collaboration. "Performance of b-jet identification in the ATLAS experiment". In: *JINST* 11 (2016), P04008. DOI: 10.1088/1748-0221/11/04/P04008. arXiv: 1512.01094 [hep-ex] (cit. on p. 7).

[11] ATLAS Collaboration. *Optimisation of the ATLAS b-tagging performance for the 2016 LHC Run*. ATL-PHYS-PUB-2016-012. URL: https://cds.cern.ch/record/2160731 (cit. on p. 7).

[12] ATLAS Collaboration. "Search for Supersymmetry in final states with missing transverse momentum and multiple b-jets in proton–proton collisions at $\sqrt{s} = 13$ TeV with the ATLAS detector". In: (2017). arXiv: 1711.01901 [hep-ex] (cit. on p. 7).

[13] ATLAS Collaboration. "Search for pair production of gluinos decaying via stop and sbottom in events with b-jets and large missing transverse momentum in pp collisions at $\sqrt{s} = 13$ TeV with the ATLAS detector". In: *Phys. Rev. D* 94 (2016), p. 032003. DOI: 10.1103/PhysRevD.94.032003. arXiv: 1605.09318 [hep-ex] (cit. on pp. 7, 11).

[14] ATLAS Collaboration. *Electron efficiency measurements with the ATLAS detector using the 2015 LHC proton–proton collision data*. ATLAS-CONF-2016-024. 2016. URL: https://cds.cern.ch/record/2157687 (cit. on p. 8).

[15] ATLAS Collaboration. "Electron and photon energy calibration with the ATLAS detector using LHC Run 1 data". In: *Eur. Phys. J. C* 74 (2014), p. 3071. DOI: 10.1140/epjc/s10052-014-3071-4. arXiv: 1407.5063 [hep-ex] (cit. on p. 8).

[16] ATLAS Collaboration. "Muon reconstruction performance of the ATLAS detector in proton–proton collision data at $\sqrt{s} = 13$ TeV". In: *Eur. Phys. J. C* 76 (2016), p. 292. DOI: 10.1140/epjc/s10052-016-4120-y. arXiv: 1603.05598 [hep-ex] (cit. on p. 8).

[17] Benjamin Nachman et al. "Jets from Jets: Re-clustering as a tool for large radius jet reconstruction and grooming at the LHC". In: *JHEP* 02 (2015), p. 075. DOI: 10.1007/JHEP02(2015)075. arXiv: 1407.2922 [hep-ph] (cit. on p. 11).

[18] ATLAS Collaboration. *Jet reclustering and close-by effects in ATLAS Run 2*. ATLAS-CONF-2017-062. 2017. URL: https://cds.cern.ch/record/2275649 (cit. on p. 11).

[19] David Krohn, Jesse Thaler, and Lian-Tao Wang. "Jet Trimming". In: *JHEP* 02 (2010), p. 084. DOI: 10.1007/JHEP02(2010)084. arXiv: 0912.1342 [hep-ph] (cit. on p. 11).

[20] ATLAS Collaboration. *Performance of Top Quark and W Boson Tagging in Run 2 with ATLAS*. ATLAS-CONF-2017-064. 2017. URL: https://cds.cern.ch/record/2281054 (cit. on p. 11).

[21] ATLAS Collaboration. *Expected performance of missing transverse momentum reconstruction for the ATLAS detector at* $\sqrt{s} = 13$ *TeV*. ATL-PHYS-PUB-2015-023. 2015. URL: https://cds.cern.ch/record/2037700 (cit. on p. 12).

[22] ATLAS Collaboration. *Performance of missing transverse momentum reconstruction with the ATLAS detector in the first proton–proton collisions at* $\sqrt{s} = 13$ *TeV*. ATL-PHYS-PUB-2015-027. 2015. URL: https://cds.cern.ch/record/2037904 (cit. on p. 12).

[23] ATLAS Collaboration. "Jet energy measurement with the ATLAS detector in proton–proton collisions at $\sqrt{s} = 7$ TeV". In: *Eur. Phys. J. C* 73 (2013), p. 2304. DOI: 10.1140/epjc/s10052-013-2304-2. arXiv: 1112.6426 [hep-ex] (cit. on p. 13).